
MOX-Report No. 51/2019

# Reduced models for liquid food packaging systems

Parolini, N.; Riccobene, C.; Schenone, E.

MOX, Dipartimento di Matematica
Politecnico di Milano, Via Bonardi 9 - 20133 Milano (Italy)

mox-dmat@polimi.it http://mox.polimi.it

# Reduced models for liquid food packaging systems

Nicola Parolini, Chiara Riccobene and Elisa Schenone

**Abstract** Simulation tools are nowadays key elements for effective production, design and maintenance processes in various industrial applications. Thanks to the advances that have been achieved in the past three decades, accurate and efficient solvers for computational fluid dynamics and computational mechanics are routinely adopted for the design of many products and systems. However, the most accurate models accounting for the complete three-dimensional complex physics (of even multi-physics) are not always the best option to pursue, in particular in the preliminary design phase or whenever very fast evaluations are required. In this paper, we present a set of reduced numerical models that have been developed in the past few years to support the design of paperboard packaging systems.

## Introduction

Food packaging is an important industrial sector in which the development of highly specialized automation systems plays a fundamental role. The entire process should be able to meet the tight standards for safety and quality control in food industry, as well as the demand of high reliability and productivity in complex industrial plants.

Laminated paperboard is a widely used material in the packaging industry, since box shaped solids can be easily obtained from flat paper roll, and the formed packages are light and stiff. The most efficient way to assemble and fill carton based boxes consists in deforming a cylindrical sleeve filled with liquid, using a jaw system in

Nicola Parolini
MOX, Dipartimento di Matematica, Politecnico di Milano, P.zza Leonardo da Vinci 32, 20133 Milano e-mail: nicola.parolini@polimi.it

Chiara Riccobene
MOXOFF s.p.a., via Schiaffino 11/19, 20159 Milano e-mail: chiara.riccobene@moxoff.com

Elisa Schenone
MOXOFF s.p.a., via Schiaffino 11/19, 20159 Milano e-mail: elisa.schenone@moxoff.com

which mechanical clamps enter periodically in contact with the carton tube squeezing it until it is closed and shaping its lateral sides to a rectangular section (see Figure 1).

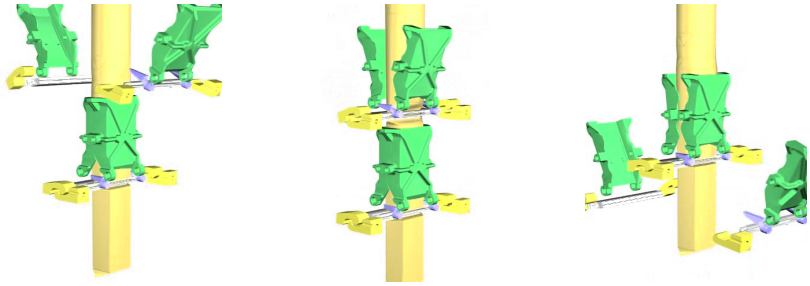

**Fig. 1** The action of the jaw system that shapes a cylindrical carton tube in boxes (courtesy of Tetra Pak Packaging Solution s.p.a.)

In this paper, we will consider a specific packaging technology, for the assembling of carton-based liquid food packages in highly performing automatized filling machines, able to assemble several packages per seconds in an aseptic environment with a fully automatic material supply.

## 1 A complex FSI problem

A filling machines is a complex system in which, starting from a roll of laminated paperboard and a continuous liquid food supply, filled bricks are assembled at a production rate of several thousands per hour. The paperboard is initially unrolled and is subject to a sterilization process crossing a peroxide bath, then is wrapped and vertically sealed in a cylindrical tube moving downward around the injector pipe. At the end of the process, which occurs around the outflow of the injector pipe, the bricks are assembled through the following steps (sketched in Figure 2):

(a) the bottom end of the package is folded and sealed;
(b) the package is laterally shaped by the jaw system;
(c) the top end of the package is closed and the bottom end is cut;
(d) the semi-finished package is released.

The fluid is injected into the carton tube through the co-axial injector pipe. The carton tube is deformed by the combined action of the jaw system and the action of the fluid, whose motion is, in turn, affected by the carton tube deformation. This coupled interaction defines a complex fluid-structure interaction (FSI) problem.

A simulation of the complete three-dimensional FSI problem coupling the incompressible Navier-Stokes equations governing the product fluid dynamics with the elasticity equations governing the structural deformation has been subject of

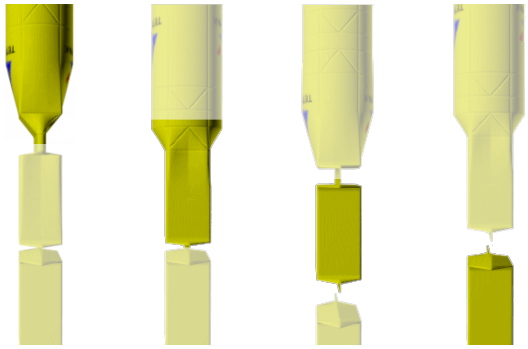


**Fig. 2** Different phases of the forming cycle: a) bottom closure b) side forming c) top closure d) package release

research for the specific application at hand (see, e.g., [21, 20, 1]), as well as applications which share some key characteristics of the considered problem, as the strongly coupled nature of the FSI coupling [8, 7, 2, 6, 16, 5, 17]. In particular, it is well known from the literature that most staggered fluid-structure interaction coupling can be subjected to numerical instabilities whenever the so-called *added mass effect* is present [3], which is most often the case when a liquid interacts with a deformable thin structure. In such conditions, a strongly coupled FSI algorithm is necessary, which typically requires a number of sub-iterations at each time step solving for the fluid and the structural problems. As a consequence, the computational cost of a full 3D FSI simulation for this kind of applications is most of the time unaffordable and resorting to reducing strategies become unavoidable.

## 2 Geometrical model reduction

A first numerical reduction approach for the filling machine has been obtained deriving a geometrical reduced mathematical model governing the fluid-structure interaction between the filling liquid and the papertube. The filling portion of the packaging system has been modeled adopting a low dimensional (1D-0D) geometrical multiscale model inspired by a similar simulation framework that has been successfully adopted in the past few years for modeling the human cardiovascular system [9, 22, 10, 11].

This kind of models can be extremely useful in the design process of the packaging machine as they allow fast (in some cases, real-time) simulations able to capture the main flow features associated to the pulsatile flow generated by the periodic contraction of the papertube. In particular, they are used to simulate the propagation of the strong pressure waves that are produced by the periodic squeezing of the

papertube by the jaw system. The objective of this kind of analyses is the design of effective tools to limit their impact on the final quality of the packages.

In this regard, two are the main technologies that are usually adopted in packaging systems: the first in which the pressure waves are dampened constraining the pulsatile flow to move across small orifices distributed on a *counter-pressure flange*; the second where the dampening effect is obtained using an *air bucket* which is periodically filled and emptied. Two sketches of the packaging systems each equipped with one of the pressure dampeners are displayed in Figure 3. For both configurations, a constant inflow is supplied by the injector, while a time dependent flowrate associated to the squeezing action of the jaw system can be prescribed at the lower boundary. Indeed, in the reduced model, we will prescribe at lower boundary the net flowrate given by the difference between the constant flowrate through the injector and the time-dependent flowrate associated to the change of volume imposed by the jaw system (that has been estimated solving the full 3D package deformation using the software Abaqus).

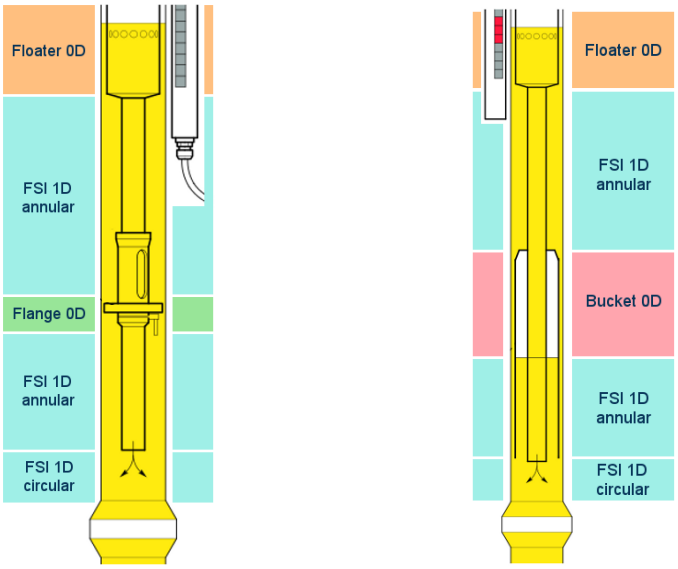


**Fig. 3** Two pressure wave dampener technologies: counter-pressure flange (left) and air bucket (right)

A set of geometrical reduced models, one for each of the sub-domains has been identified, together with suitable coupling and boundary conditions.

In order to model the machine equipped with the flange (Figure 3, left), we need to define a 1D model governing the flow in the cylindrical domain under the injector, a similar 1D model for the flow in the annular domains around the injector and 0D models accounting for the flange and the floater. These model are accommodated in

series and the coupling conditions impose the continuity of flowrate and pressure at the interface between different models.

A similar model coupling 1D and 0D elements has been developed for the machine equipped with the air bucket (Figure 3, right). Also in this case, 1D FSI models for circular and annular sections are required, while the air bucket and the floater are modeled by 0D models. In this case, the flowrate is imposed on the bottom surface is split between a portion that enters the bucket (changing the liquid level inside it and, therefore, the pressure of the enclosed air) and the remaining part that flows through the thin annular interspace between the bucket and the papertube. Thus, in this case, the coupling condition should also account for this flow bifurcation by prescribing a balance of flowrates and the continuity of pressure at the bifurcation point.

Note that, in order to impose the coupling conditions at each time step of the numerical solution, the different models may be solved iteratively until continuity of pressure and flowrate is achieved at each interface (see [19]).

For both configurations, the flowrate in imposed on the bottom boundary while a pressure boundary condition (accounting for the hydrostatic level) is imposed on the upper boundary. As will be discussed in Section 2.1, this choice of boundary conditions is consistent with the hyperbolic nature of the 1D models.

Hereafter, we briefly describe the different 1D and 0D models that are used for the two types of systems (flange and bucket), starting from the mono-dimensional FSI models that govern the flow within the deformable papertube.

## 2.1 1D FSI model

Mono-dimensional FSI models for incompressible flows interacting with elastic vessels have been developed and extensively used for the simulation of the human cardiovascular system (see, *e.g.*, [9, 22, 11]). These models work under the assumptions of axial symmetry, small displacement of the structure (usually limited to normal direction), dominance of the axial component. Under this hypotheses, by integrating the incompressible Navier-Stokes equations over the cross section and introducing a simplified (algebraic) model for the elastic response of the structure, a system of partial differential equations can be derived for $z \in \Omega \subset \mathbb{R}, t > 0$, namely:

$$\frac{\partial A}{\partial t} + \frac{\partial Q}{\partial z} = 0, \tag{1a}$$

$$\frac{\partial Q}{\partial t} + \frac{\partial}{\partial z}\left(\alpha \frac{Q^2}{A}\right) + \frac{A}{\rho}\frac{\partial p}{\partial z} + K_r\left(\alpha \frac{Q}{A}\right) + Ag = 0. \tag{1b}$$

where $A(z,t)$ is the section area at longitudinal position $z$ at time $t$, $Q(z,t)$ is the flowrate, $p(z,t)$ is the mean pressure on the section, $\alpha$ is the Coriolis coefficient (which depends on the velocity profile over the section), $K_r$ is a friction coefficient and $g$ is a specific body force (most often the gravity acceleration). In the simplest

case, for cylindrical domains, the structural response can be described by an algebraic relation between the pressure difference across the structure and the normal displacement $\eta$,

$$p - p_{\text{ext}} = b\eta,$$

where $p_{\text{ext}}$ is the prescribed pressure distribution on the external side of the structure and the stiffness parameter $b$ is defined as

$$b = \frac{Eh}{(1-\xi^2)R_0^2}, \tag{2}$$

with $E$ and $\xi$ denoting the Young modulus and the Poisson ratio of the material, respectively, $h$ its thickness and $R_0$ is the radius of the reference (initial) configuration.

In order to close system (1), the structural response can be more conveniently formulated as an algebraic relation between the flow pressure $p$ and the area $A$ given by

$$p - p_{\text{ext}} = \psi(A; A_0, \beta);$$

where $A_0 = \pi R_0^2$ and $\beta$ is a stiffness parameter. The exact definition of $\psi$ and $\beta$ will be detailed in the following for the different domain geometries (circular or annular).

System (1) is an hyperbolic system for the conservative variables $(A, Q)$ that is here numerically solved using a finite element Taylor-Galerkin method [9]. The characteristic analysis of system (1), that has been carried out in [22], shows that, for the case at hand, the Jacobian matrix has one positive eigenvalue, corresponding to a characteristic wave moving in positive $z$ direction and a negative one, corresponding to a second characteristic wave moving backwards. Therefore, one boundary condition has to be imposed on each boundary of the 1D domain.

### 2.1.1 Closure for circular sections

For circular sections, the normal displacement is defined as $\eta = R - R_0 = \frac{\sqrt{A}-\sqrt{A_0}}{\sqrt{\pi}}$, so that the closure of the 1D model (1) can be obtained (as in [11]), by choosing

$$\psi(A; A_0, \beta) = \beta(\sqrt{A} - \sqrt{A_0}), \tag{3}$$

where the stiffness coefficient is given by

$$\beta = \frac{\sqrt{\pi}Eh}{(1-\xi^2)A_0}. \tag{4}$$

The Coriolis coefficient $\alpha$ is defined as follows

$$\alpha = \frac{\int_S s^2 d\sigma}{A},$$

where we consider an axisymmetric velocity profile $s(r)$ over the section $S$ as the power law radial function $s(r) = \gamma^{-1}(\gamma+2)(1-(r/R)^{\gamma})$. The friction coefficient can be defined as

$$K_r = -2\pi\nu s'(1) = 2\pi\nu(\gamma+2),$$

where $\nu$ is the kinematic viscosity of the fluid,

For $\gamma = 2$, we have a parabolic profile which gives $\alpha = 4/3$ and $K_r = 8\pi\nu$, while for the typical choice $\gamma = 9$, we get $\alpha = 1.1$ and $K_r = 22\pi\nu$.

### 2.1.2 Closure for annular domain

In order to consider the annular subdomains around the injector and the paper tube, a similar 1D model has been developed. Here the area of the annular section is given by $A = \pi(R^2 - R_i^2)$, where $R_i$ denotes the internal radius on the annulus. Similarly, the area of the reference section is $A_0 = \pi(R_0^2 - R_i^2)$.

To close system (1) we define the normal displacement as $\eta = R - R_0 = \frac{\sqrt{A+A_i}-\sqrt{A_0+A_i}}{\sqrt{\pi}}$, where $A_i = \pi R_i^2$, and we obtain:

$$\psi(A; A_0, \beta) = \beta(\sqrt{A + A_i} - \sqrt{A_0 + A_i}) \tag{5}$$

with $\beta$ defined as in (4).

In this case the Coriolis and friction coefficients are computed assuming an axisymmetric parabolic profile on the annular section, namely $s(r) = ar^2 + br + c$ with $a = -\frac{4}{(R_0-R_i)^2}$, $b = -(R_0 + R_i)a$ and $c = -aR_i^2 - bR_i$.

## 2.2 0D model of the counter-pressure flange

The contribution of the counter-pressure flange is accounted for with a 0D lumped model, prescribing a concentrated pressure loss as a function of the flowrate. The flange works as a pressure wave dampener thanks to the dissipation occurring on the flow which is confined in a number of small orifices distributed on the flange surface. The orifices are usually designed such that the loss coefficient for the flow moving upwards is larger than the one for the recovery phase when the flow is moving downward across the flange. Assuming $N$ identical orifices on the flange, the 0D flange model is given by:

$$\Delta p = p_{\text{under}} - p_{\text{over}} = \frac{1}{2}\rho\,\text{sign}(Q)\left(\frac{Q}{N\,A_i}\right)^2 C_d, \tag{6}$$

where $\Delta p$ is the pressure difference across the flange (positive for upwards flowrate), $A_i$ is the area of single orifice and $C_d$ is the pressure loss coefficient (that needs to be estimated).

## 2.3 0D model of the air bucket

Air buckets are typically used in packaging system with higher production rates. In this case the dampening effect is given by the combined action of the energy absorbed by the gas inside the bucket which is periodically compressed and the viscous dissipation occurring on the liquid flowing in the tiny annular domain between the bucket and the papertube (see Figure 3).

A 0D model computing the gas pressure inside the bucket is obtained considering the ideal gas law ($pV = \text{const}$) and computing the gas volume by updating the liquid level inside the bucket as a function of the flowrate entering the bucket, namely

$$h_l(t) = \left( h_0 + \frac{1}{A_b} \int_0^t Q_b \, d\tau \right), \tag{7}$$

where $h_0$ is the initial level of liquid in the bucket, $A_b$ is the area of the section of the bucket and $Q_b$ is the flowrate entering the bucket. Indicating with $L$ the length of the bucket, the volume of the gas inside the bucket is $V(t) = A_b(L - h_l(t))$.

An additional 0D model accounting for the floater can be added to the system. As sketched in Figure (3), the floater is a light coaxial cylinder placed above the pressure dampener and moving vertically along the injector, used to measure the level of liquid inside the papertube during the different phases of the filling cycle. Even if ideally the floater should move with the free-surface level, due to the strong inertia associated to the fast level variations, a model able to capture the dynamics of the floater is required. Indeed, the dynamics of the floater seems to play an additional (non negligible) role in the pressure wave dampening and including it in the model can be useful to take into account these effects.

## 2.4 Numerical results of the geometrical reduced FSI models

For the problem at hand, some of the hypotheses that have been introduced to derive the geometrical reduced models are not completely fulfilled (for instance, close to the injector the transverse velocity components may not be negligible). However, the reduce models introduced in the previous section have proved to be able to to capture the main flow features of the system, in particular concerning the pressure wave propagation.

These models have been adopted to simulate a number of different packaging machines of both types. In Figure 4 (left), we compare, for a machine with the counter-pressure flange, the numerical prediction and the experimental measurements of the time evolution over two periods of the pressure level under the flange. We can observe that amplitude and phase of the two main pressure peaks are well approximated. For confidentiality limitations, the pressure scale has been removed.

Similar results, also showing an good matching between the numerical results and the experimental measurements, have been obtained for air bucket systems. In Figure 4 (right), the comparison related to the gas pressure inside the bucket is displayed.

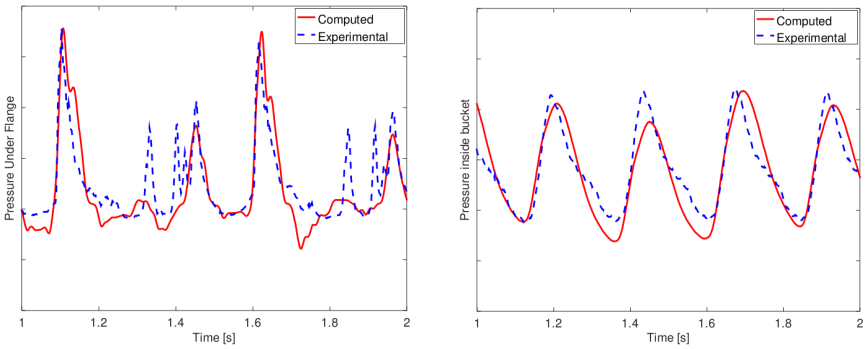


**Fig. 4** Comparison with experimental measurements for the pressure drop across the flange (left) and the gas pressure inside the bucket (right)

## 3 Reduced 3D FSI using transpiration and absorbing BCs

As we have seen, the geometrical reduction represents a possible reduction strategy allowing to capture some relevant characteristics of the coupled system. However, some aspects of the problem can only be captured resorting to the simulation of the complete flow field in 3D.

Since, we have seen that the solution of a complete 3D FSI problem may be prohibitively expensive due to the need of a strongly coupled FSI approach, it is worth trying to devise a simulation framework for FSI simulation with an intermediate level of complexity. In this respect, the interaction between the fluid and the deformable walls may be modeled by the so-called *transpiration boundary conditions*. As in[4, 12], for small displacements, the wall structural response can be modeled as an elastic shell where the tangential components of the wall stress and of the displacement are neglected. The main advantage of this approach, that has been extensively exploited in aeronautical applications to solve aero-elastic problems, is that it does not require to change the domain (and thus to move the computational grid) at each time step and the simplified structural model reduces to a boundary condition for the flow problem.

Assuming that the displacement $\eta$ is only in the normal direction, following the derivation proposed in [4], the transpiration condition can be derived from an elasto-dynamic equation for $\eta$ on $\Sigma$ and can be formulated as a Robin-type boundary condition for the normal component of the velocity in the time-dependent Navier-Stokes equations, as follows:

$$\begin{cases} \partial_t \mathbf{u} - \nu \nabla^2 \mathbf{u} + (\mathbf{u} \cdot \nabla)\mathbf{u} + \nabla p = \mathbf{f}, & \text{in } \Omega \times (0,T), \\ \nabla \cdot \mathbf{u} = 0, & \text{in } \Omega \times (0,T), \\ \mathbf{u} = \mathbf{u}_0, & \text{in } \Omega, t = 0, \\ \mathbf{u} = \mathbf{u}_{\text{in}}, & \text{on } \Gamma_{\text{in}} \times (0,T), \\ -\nu \partial_{\mathbf{n}} \mathbf{u} + p\mathbf{n} = 0, & \text{on } \Gamma_{\text{out}} \times (0,T), \\ \mathbf{u} \times \mathbf{n} = 0, & \text{on } \Sigma \times (0,T), \\ \rho_s h \partial_t \mathbf{u} \cdot \mathbf{n} - \nabla_c \cdot (\mathbf{T} \nabla_c \eta) + a\mathbf{u} \cdot \mathbf{n} + b\eta = p, & \text{on } \Sigma \times (0,T), \end{cases} \tag{8}$$

where $\mathbf{u}$ is the fluid velocity, $p$ is the fluid pressure (rescaled with the fluid density), $\nu$ is the fluid kinematic viscosity, $\rho_s$ is the structure density, $h$ is the structure thickness, $\nabla_c$ is the covariant gradient, $T$ is the stress (possibly prestressed) tensor, $a$ and $b$ are damping and elastic coefficients, respectively (see [4] for details).

The normal displacement $\eta$ can be computed integrating over time the normal velocity, as

$$\eta := \int_0^t \mathbf{u} \cdot \mathbf{n} ds.$$

The coefficient $b$ depends on the material properties of the deforming structure and characterize its elastic response: the greater $b$ is, the more rigid the structure. In particular, for cylindrical structures, $b$ can be defined as in Equation (2).

Further simplification of the structural model may be considered when projection-based flow solvers are used, resulting on a pressure boundary condition on the moving wall, as discussed in [12].

A numerical solution of Problem (8) has been obtained using $\mathbb{P}_2/\mathbb{P}_1$ finite element for velocity and pressure and using an implicit Euler time advancing scheme with a semi-implicit treatment of the convective term.

The ability of the model in capturing the propagation of the pressure wave generated by the time-dependent inlet velocity profile $\mathbf{u}_{\text{in}}(t)$ has been investigated. In order to avoid (or at least minimize) the numerical wave reflection that are generated when homogeneous Neumann condition are imposed on the outflow boundary, the linearized absorbing condition (LAC) proposed in [14] is imposed at the outflow boundary. This condition prescribe a linear dependence of the pressure on the flow rate $Q$:

$$p = \frac{\pi \sqrt{b}}{\sqrt{2\rho} A^{5/4}} Q \qquad \text{on } \Gamma_{\text{out}}, \tag{9}$$

where $A$ is the area of the outflow boundary.

A simple test case to assess the reduced 3D FSI model with transpiration and absorbing boundary conditions has been setup. We consider the propagation of a pressure wave in the flange system. We start from the fluid at rest, an hydrostatic pressure distribution and null flowrate imposed on the bottom boundary. At a given time $t = \bar{t}$, a sinusoidal pulse on the inlet flowrate is started, which causes a pressure wave to propagate along the papertube domain, thanks to the deformability of the wall accounted for by the transpiration conditions.

In Figure 5, the solution obtained on a longer domain are compared with two solutions on a shorter domain with and without absorbing boundary conditions. The

effectiveness of the linearized absorbing condition in reducing the spurious reflection at the outflow boundary can be clearly appreciated.

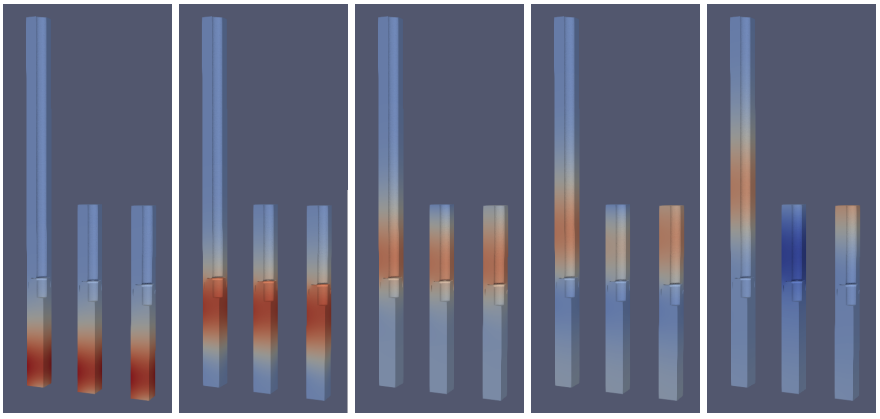


**Fig. 5** Propagation of the pressure wave at different time instants. For each time, the solution obtained on a longer domain (left), with homogeneous Neumann outflow condition (middle) and with the linear absorbing condition (right) are reported

A second test case is presented in order to highlight the importance of accounting for FSI effects in this kind of problems, even if with simplified approach as the one based on transpiration boundary conditions. In Figure 6, we compare the different behaviors of the pressure for different values of the wall rigidities ($E = 5 \times 10^9$ GPa and $E = 5 \times 10^{10}$ GPa). The peaks on the pressure drop across the flange is almost doubling when the higher stiffness is considered and the pressure wave travels much faster. With this results in mind, it is clear that no meaningful indication on the pressure can be obtained when simulating the problem with rigid CFD simulations that do not account, at any level of details, for FSI effects.

## 4 Reduced order modeling for multi-query problems

A further possible reduction approach that is currently being investigated for the considered application is based on reduced order models (ROM), such as the Reduced Basis (RB) method [18, 23, 13] or the Proper Orthogonal Decomposition (POD) method [15, 24]. These approaches are particularly interesting when multi-query problems are considered, that is when a large number of CFD evaluations on the 3D geometry are required (such as, for instance, parametric, optimization or uncertainty quantification studies). In all reduced order models, the approximate solutions can be computed very efficiently (sometime in real time) as a suitable (linear or nonlinear) combination of ad-hoc basis functions. The latter are pre-computed in a (computa-

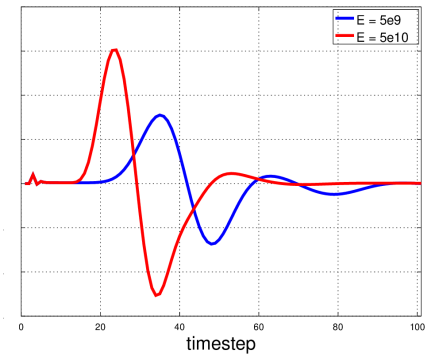


**Fig. 6** Time history of the pressure drop on the flange for different values of Young modulus

tionally expensive) offline phase by solving the high fidelity problem for a limited set of parameters.

In the application at hand, preliminary results have been obtained on the fluid-dynamic analysis of the counter-pressure flange. This kind of analyses can be used, for instance, to obtain the pressure/flowrate characterization for various design parameters in order to evaluate the pressure drop coefficient to be used in the 0D model described in Section 2.2.

A parametric study considering two parameters (fluid viscosity and papertube diameter) has been carried on using a reduced basis method and taking as basis functions the first 10 modes obtained by a POD computed on 24 snapshots uniformly distributed in the parameter space. In Figure 7, we report a comparison between the velocity and pressure field computed using a high fidelity finite-element solver and the corresponding reduced solution. The relative error for the solution obtained with a choice of parameters different from those used for the snapshots shows that the reduced solution is able to guarantee a good accuracy. The advantage in terms of computational cost can be appreciated comparing the CPU time required for the high fidelity finite-element solution (4.5 hours) with that of the online phase of the reduced method (7.3 minutes).

## Concluding remarks

We have presented a set of numerical simulation tools that have been developed to support the design of packaging systems for liquid food products. Different reduction strategies, ranging from geometrical reduction, to a simplified treatment of 3D FSI problems based on transpiration wall conditions and including reduced order models for multi-query problems, have been developed and effectively integrated in

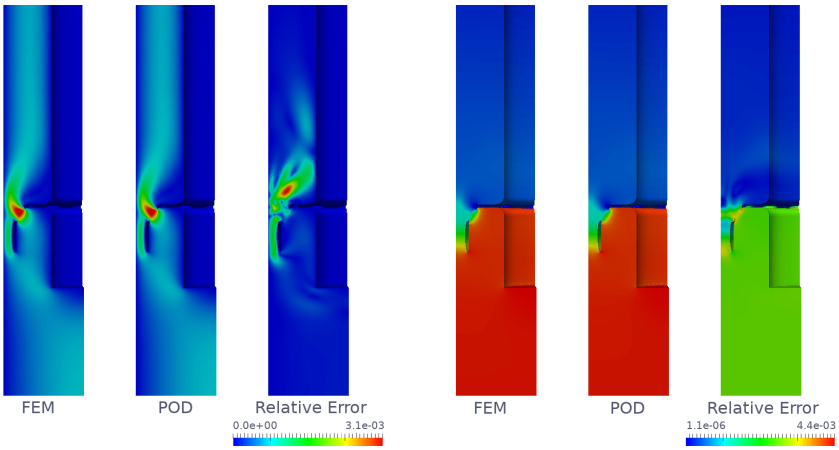


**Fig. 7** Comparison of the velocity (left) and pressure (right) fields: for each field the high fidelity FEM solution, the POD solution and the relative error are reported (from left to right).

a complex design framework, in which the role of numerical simulations, at all levels of computational complexities, plays an increasingly important role.

**Acknowledgements** This research has been supported by Tetra Pak Packaging Solution s.p.a. in the framework of a consolidated research partnership with MOXOFF s.p.a and the MOX Laboratory. The authors are grateful to all the members of Tetra Pak technical team, leaded by Dr. Roberto Borsari, for the insightful and stimulating discussions. Marco Pischedda, Andrea Mola and Jacopo Corno are also acknowledged for their contribution on the development of the tools presented in this work.

## References

1. L. Andersson. Numerical Investigations of a Partitioned FSI Algorithm for Tetra Pak's Filling Tube. Master's thesis, Lund University, 2016.
2. S. Badia, A. Quaini, and A. Quarteroni. Modular vs. non-modular preconditioners for fluid-structure systems with large added-mass effect. *Comput. Methods Appl. Mech. Engrg.*, 197(49-50):4216–4232, 2008.
3. P. Causin, J.-F. Gerbeau, and F. Nobile. Added-mass effect in the design of partitioned algorithms for fluid-structure problems. *Comput. Methods Appl. Mech. Engrg.*, 194(42-44):4506–4527, 2005.
4. T. Chacón Rebollo, V. Girault, F. Murat, and O. Pironneau. Analysis of a coupled fluid-structure model with applications to hemodynamics. *SIAM Journal on Numerical Analysis*, 54(2):994–1019, 2016.
5. C. Colciago, S. Deparis, and A. Quarteroni. Comparisons between reduced order models and full 3D models for fluid–structure interaction problems in haemodynamics. *J. Comput. Appl. Math.*, 265(0):120 – 138, 2014.
6. P. Crosetto, S. Deparis, G. Fourestey, and A. Quarteroni. Parallel algorithms for fluid-structure interaction problems in Haemodynamics. *SIAM J. Sci. Comput.*, 33(4):1598–1622, 2011.

7. S. Deparis, M. Discacciati, G. Fourestey, and A. Quarteroni. Fluid-structure algorithms based on Steklov-Poincaré operators. *Comput. Methods Appl. Mech. Engrg.*, 195(41-43):5797–5812, 2006.
8. L. Formaggia, J. F. Gerbeau, F. Nobile, and A. Quarteroni. On the coupling of 3d and 1d navier-stokes equations for flow problems in compliant vessels. *Computer Methods in Applied Mechanics and Engineering*, 191(6-7):561 – 582, 2001.
9. L. Formaggia, D. Lamponi, and A. Quarteroni. One-dimensional models for blood flow in arteries. *Journal of Engineering Mathematics*, 47(3):251–276, 2003.
10. L. Formaggia, A. Moura, and F. Nobile. On the stability of the coupling of 3d and 1d fluid-structure interaction models for blood flow simulations. *ESAIM: Mathematical Modelling and Numerical Analysis*, 41(4):743âĂŞ769, 2007.
11. L. Formaggia, Q. Quarteroni, and A. Veneziani. Cardiovascular mathematics : modeling and simulation of the circulatory system. Springer, 2009.
12. K. P. Gostaf and O. Pironneau. Pressure boundary conditions for blood flows. *Chinese Annals of Mathematics, Series B*, 36(5):829–842, 2015.
13. Jan S. Hesthaven, Gianluigi Rozza, and Benjamin Stamm. *Certified Reduced Basis Methods for Parametrized Partial Differential Equations*. Springer Briefs in Mathematics. Springer, Switzerland, 1 edition, 2015.
14. J. Janela, A. Moura, and A. Sequeira. Absorbing boundary conditions for a 3d non-newtonian fluid–structure interaction model for blood flow in arteries. *International Journal of Engineering Science*, 48(11):1332–1349, 2010.
15. K. Kunisch and S. Volkwein. Galerkin proper orthogonal decomposition methods for parabolic problems. *Numerische Mathematik*, 90(1):117–148, 2001.
16. M. Lombardi, M. Cremonesi, A. Giampieri, N. Parolini, and A. Quarteroni. A strongly coupled fluid-structure interaction model for wind-sail simulation. In *4th High Performance Yacht Design Conference 2012, HPYD 2012*, 2012.
17. M. Lombardi, N. Parolini, and A. Quarteroni. Radial basis functions for inter-grid interpolation and mesh motion in {FSI} problems. *Computer Methods in Applied Mechanics and Engineering*, 256:117 – 131, 2013.
18. Y. Maday and E. M. Ronquist. A reduced-basis element method. *Journal of scientific computing*, 17(1):447–459, 2002.
19. A. C. Malossi, B. J. Blanco, S. Deparis, and A. Quarteroni. Algorithms for the partitioned solution of weakly coupled fluid models for cardiovascular flows. *Int. J. Numer. Meth. Biomed. Engng*, 27:2035–2057, 2011.
20. A. Mameli, A. Magnusson, A. Aksenov, K. Kuznetsov, T. Luniewski, and I. Moskalev. Simulating the pouch forming process using a detailed fluid-structure interaction. In *Proceedings of the 2013 SIMULIA Customer Conference*, pages 1–15, 2013.
21. M. Olsson, A. Magnusson, and S. C. Prasad. Simulation of the forming process of liquid filled packages using coupled eulerian-lagrangian approach. In *Proceedings of the 2009 SIMULIA Customer Conference*, pages 1–12, 2013.
22. A. Quarteroni and L. Formaggia. *Mathematical modelling and numerical simulation of the cardiovascular system,* Computational models for the human body*, Handbook of numerical analysis series Volume XII*. N. Ayache Guest Ed. and P. G. Ciarlet Ed., Elsevier, 2004.
23. A. Quarteroni, A. Manzoni, and F. Negri. *Reduced Basis Methods for Partial Differential Equations: An Introduction*. UNITEXT. Springer International Publishing, 2015.
24. M. Rathinam and L. R. Petzold. A new look at proper orthogonal decomposition. *Journal on Numerical Analysis*, 41(5):1893–1925, 2004.

# MOX Technical Reports, last issues

Dipartimento di Matematica
Politecnico di Milano, Via Bonardi 9 - 20133 Milano (Italy)

**50/2019** Lusi, V.; Moore, T. L.; Laurino, F.; Coclite, A.; Perreira, R.; Rizzuti, I.; Palomba, R.; Zunino, P
*A tissue chamber chip for assessing nanoparticle mobility in the extravascular space*

**49/2019** Cicchetti, A.; Laurino, F.; Possenti, L.; Rancati, T.; Zunino, P.
*In silico model of the early effects of radiation therapy on the microcirculation and the surrounding tissues*

**46/2019** Di Iorio, J.; Vantini, S.
*funBI: a Biclustering Algorithm for Functional Data*

**47/2019** Spreafico, M.; Ieva, F.
*Dynamic monitoring of the effects of adherence to medication on survival in Heart Failure patients: a joint modelling approach exploiting time-varying covariates*

**48/2019** Di Gregorio, S.; Fedele, M.; Pontone, G.; Corno, A.F.; Zunino, P.; Vergara, C.; Quarteroni, A.
*A multiscale computational model of myocardial perfusion in the human heart*

**45/2019** Regazzoni, F.; Dedè, L.; Quarteroni, A.
*Active force generation in cardiac muscle cells: mathematical modeling and numerical simulation of the actin-myosin interaction*

**44/2019** Formaggia, L.; Gatti, F.; Zonca, S.
*An XFEM/DG approach for fluid-structure interaction problems with contact*

**41/2019** Abbà, A.; Bonaventura, L.; Recanati, A.; Tugnoli, M.;
*Dynamical p-adaptivity for LES of compressible flows in a high order DG framework*

**42/2019** Martino, A.; Guatteri, G.; Paganoni, A.M.
*hmmhdd Package: Hidden Markov Model for High Dimensional Data*

**43/2019** Antonietti, P.F.; Mazzieri, I.; Migliorini, F.
*A space-time discontinuous Galerkin method for the elastic wave equation*